JACS
JOURNAL OF THE AMERICAN CHEMICAL SOCIETY

Article

pubs.acs.org/JACS

Structure-Based Design of Functional Amyloid Materials

Dan Li,[†,‡] Eric M. Jones,[†,‡] Michael R. Sawaya,[†,‡] Hiroyasu Furukawa,[†,∥] Fang Luo,[⊥] Magdalena Ivanova,[†,‡,#] Stuart A. Sievers,[†,‡,▽] Wenyuan Wang,[⊥] Omar M. Yaghi,[†,∥] Cong Liu,[⊥] and David S. Eisenberg*[,†,‡,§]

[†]UCLA-DOE Institute, and Department of Chemistry and Biochemistry, University of California, Los Angeles, California 90095, United States

[‡]Molecular Biology Institute and [§]Howard Hughes Medical Institute, University of California, Los Angeles, California 90095, United States

[∥]Department of Chemistry, University of California-Berkeley, Materials Sciences Division, Lawrence Berkeley National Laboratory, Kavli Energy NanoSciences Institute at Berkeley, Berkeley, California 94720, United States

[⊥]Interdisciplinary Research Center on Biology and Chemistry, Shanghai Institute of Organic Chemistry, Chinese Academy of Sciences, Shanghai 200032, China

Supporting Information

ABSTRACT: Amyloid fibers, once exclusively associated with disease, are acquiring utility as a class of biological nanomaterials. Here we introduce a method that utilizes the atomic structures of amyloid peptides, to design materials with versatile applications. As a model application, we designed amyloid fibers capable of capturing carbon dioxide from flue gas, to address the global problem of excess anthropogenic carbon dioxide. By measuring dynamic separation of carbon dioxide from nitrogen, we show that fibers with designed amino acid sequences double the carbon dioxide binding capacity of the previously reported fiber formed by VQIVYK from Tau protein. In a second application, we designed fibers that facilitate retroviral gene transfer. By measuring lentiviral transduction, we show that designed fibers exceed the efficiency of polybrene, a commonly used enhancer of transduction. The same procedures can be adapted to the design of countless other amyloid materials with a variety of properties and uses.

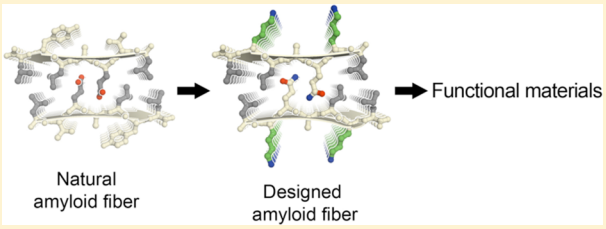

INTRODUCTION

Many proteins are capable of converting to amyloid fibers at high concentration under destabilizing conditions.[1,2] While folded proteins present extremely diverse structures, when converted to the amyloid state, they all share a uniform morphology: elongated and unbranched with widths of 8−30 nm and lengths up to several micrometers.[3] At the molecular level, amyloid fibers also share similar structures. The protofilaments that twist around one another to form the fiber are generally composed of pairs of β-sheets.[4] The sheets are parallel to the fiber axis, with the strands that are hydrogen-bonded into the sheets most often perpendicular ("in-register") but in rare cases at an angle to the axis ("out of register").[5,6] Amyloid fibers are mechanically stiff with Young's moduli ranging from 0.2 to 20 GPa, comparable with silk.[7,8] These characteristics have attracted scientists to consider them as a class of designable bio-nanomaterials with new functions.[7,9−11] To date, amyloid fibers have been functionalized for applications in tissue engineering,[12,13] drug delivery,[14−16] enzyme immobilization,[17] metal nanowires,[18−20] protein films,[21] light-harvesting nanodevices,[8,22] retroviral gene transfer enhancer,[23] environmental carbon dioxide capture,[24] and enzyme-like catalysis.[25]

Although first identified as pathological entities, amyloid fibers have evolved in living organisms from prokaryotes to eukaryotes to perform diverse functions, including signal transduction,[26] RNA granule formation,[27] memory persistence,[28] hormone storage,[29] and cell surface adhesion.[30] The distinctive properties of amyloid fibers and their diverse functions in nature suggest that research on amyloid materials could contribute significantly to bio-nanotechnology. However, the challenges include (i) identifying protein segments with high potential for forming amyloid fibers, (ii) controlling the amyloid formation, and (iii) fine-tuning the design at the molecular level to achieve an accurate performance for the application of interest.[9,11,31]

Here we propose a general method for the design of functional amyloid, based on the growing structure database of amyloid-forming peptides. Structure-based design has been an efficient method for finding molecules that interfere with protein activities and interactions. We expand the concept from soluble proteins to insoluble amyloid, from inhibition to functionalization, and from drugs to new materials. We

Received: September 18, 2014
Published: December 4, 2014

   dx.doi.org/10.1021/ja509648u | J. Am. Chem. Soc. 2014, 136, 18044−18051

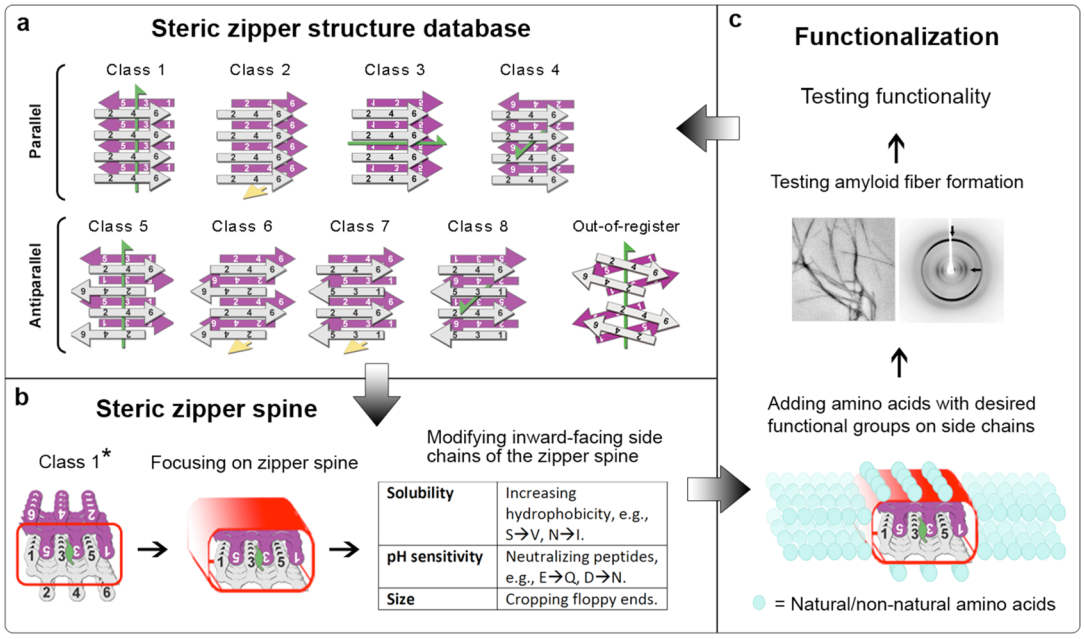

Figure 1. Concept and workflow of structure-based design of amyloid fibers with novel functions. (a) In-register zippers (8 classes) and out-of-register zippers β-sheets can be either parallel or antiparallel. Diverse geometries are available to meet the requirement of functional design. Adapted from ref 37. (b) Optimization of steric zipper spines. The inward-facing side chains of zipper spines must interdigitate for zipper formation. Before functionalization, the zipper spines are modified taking consideration of peptide solubility, pH sensitivity, and peptide size. * The Class 1 spine is illustrated here. (c) Fibers are functionalized by replacing outward-facing side chains on the zipper spine and extension of termini with functional amino acids. The designed peptides are tested for amyloid fiber formation and functionality. The performance of designed fibers can be further improved in further cycles of design and testing.

illustrate the method with two applications that demonstrate the potency of the method of design: in one, we double the capture capacity of carbon dioxide by amyloid fibers; in the other, we triple the efficiency of gene transfer by amyloid fibers.

EXPERIMENTAL SECTION

1. Peptide Crystal Structure Determination. IFQINS crystals were grown at room temperature by dissolving the peptide in water at 3 mg mL^{-1} concentration. Crystals were grown by hanging drop vaporization, mixing peptide in a 1:1 ratio with reservoir containing 3.0 M sodium chloride, and 0.1 M Bis-Tris pH 6.5.

TGVTAVA crystals were grown at room temperature by dissolving the peptide in water at 5 mg mL^{-1} concentration. Crystals were grown by hanging drop vaporization, mixing peptide in a 1:1 ratio with reservoir containing 0.2 M magnesium formate.

VVTGVTA crystals were grown at room temperature by dissolving the peptide in water at 5 mg mL^{-1} concentration. Crystals were grown by hanging drop vaporization, mixing peptide in a 1:1 ratio with reservoir containing 125 μL of isopropanol (use positive displacement pipet), 825 μL of water, and 50 μL of 1 M sodium cacodylate pH 6.5.

X-ray diffraction data sets were collected at ESRF beamline ID13, equipped with a MAR CCD detector.[32] Data were collected in 5° wedges at a wavelength of 0.9466 Å using a 5 μm beam size. The crystals were cryo-cooled (100 K) for data collection. Data were processed and reduced using Denzo/Scalepack from the HKL suite of programs.[33]

Molecular replacement solutions were obtained using the program Phaser.[34] The search models consisted of geometrically idealized β-strands with side chain conformations modeled as the most frequently observed rotamer defined in the graphics program COOT.[35] Crystallographic refinements were performed with the program REFMAC.[36] Model building was performed using COOT. Data processing and refinement statistics are reported in Supporting Information (SI) Table S1.

2. Amyloid Fiber Spine Modeling. The models of designed fibers were generated using the crystal structures of natural peptides (PDB IDs: 2ON9, 2OMM, 4R0P, 3HYD, 4R0U, 4R0W, 3Q2X, and 3OW9) as templates. Extending termini uses ideal β-strand ϕ/ψ angles. The extended terminal residues were mutated to lysine side chains. Rotamers were selected to avoid steric clash. Modeling was performed using the program COOT. Replacement of original residues to lysines was created by mutating residues to lysines in COOT. Rotamers were selected to avoid steric clashes. The model was illustrated using PYMOL (www.pymol.org).

3. Amyloid Fiber Formation. Peptides were custom-synthesized by Celtek Peptides (Franklin, TN) and GL Biochem (Shanghai) with purity over 95%. All peptides were synthesized with N-terminal acetylation and C-terminal amidation; 5 mM designed peptides were used for fiber screening, 50 mM sodium phosphate titrated with sodium hydroxide or hydrochloride to the desired pH was used as growth buffer, and 0.2 M sodium chloride was used for salt screening. Peptide solutions were incubated at 37 °C with agitation for 7−10 days. Fiber formation was monitored by TEM. Fibers were collected by centrifugation at 36320*g* for 20 min, and were resuspended with the growth buffer. For carbon dioxide capture, the fiber suspension was lyophilized until the sample became a white powder.

4. Transmission Electron Microscopy (TEM). Each sample (5 μL) was spotted directly onto freshly glow-discharged carbon-coated electron microscopy grids (Ted Pella, Redding, CA). After 3 min incubation, grids were rinsed twice with 5 μL of distilled water and stained with 1% wt/vol uranyl acetate for 1 min. Specimens were examined in a JEM1200-EX electron microscope at an accelerating voltage of 120 kV, and a Tecnai G2 Spirit electron microscope operated at an accelerating voltage of 120 kV. Images were recorded digitally by wide angle (top mount) BioScan 600 W 1×1K digital camera (Gatan, Pleasanton, CA), and a 4×4K charge-coupled device camera (BM-Eagle, FEI).

5. Circular Dichroism (CD) Spectroscopy. CD Spectra were acquired using a JASCO J-715 spectrometer equipped with a JASCO PTC-348 temperature controller. Measurements were made at 23 °C. Far-UV spectra (260−190 nm) were collected in 0.1 cm path-length quartz cells with fiber pellets suspended in water. Raw data were

dx.doi.org/10.1021/ja509648u | J. Am. Chem. Soc. 2014, 136, 18044−18051

Table 1. Summary of Our Peptide Designs for Carbon Dioxide Capture

natural peptide	source protein	geometry	buried surface[a] (Å)	Sc[a]	zipper spine[b]	modified spine	designed peptide	hydrophobicity[c]	fiber yield
VQIVYK	Tau	parallel	392	0.764	VxIxY	VxIxY	VKIVYK[24]	0.133	++
							VQIVYKK[24]	−0.007	++
GNNQQNY	Sup35	parallel	542	0.859	NxQxN	NxQxN	KNNQKNY	−0.847	+
IFQINS	lysozyme	parallel	564	0.787	FxIxS	FxIxV	IFKINVK	0.179	++
LVEALYL	insulin	parallel	726	0.798	LxExLxL	LxQxLxL	LKQALKL	−0.007	++
TGVTAVA	α-Syn	parallel	548	0.873	VxAxA	VxAxA	VKAVAK	0.067	++
VVTGVTA	α-Syn	parallel	568	0.924	VxGxT	VxGxT	VVKGVTK	0.096	++
NKGAII	Aβ	parallel	625	0.862	NxGxI	NxGxI	NKGAIK	−0.217	−
						IxGxI	IKGAIK	0.143	+
KLVFFA	Aβ	antiparallel	238	0.348	LVFF	LVFF	KLVFFAK[d]	0.306	++

[a]Values are calculated from PDB IDs 2ON9, 2OMM, 4R0P, 3HYD, 4R0U, 4R0W, 3Q2X, and 3OW9. [b]"x" represents any amino acids. [c]Hydrophobicity is calculated as the sum of hydrophobicity values[47] of all the amino acids, divided by the number of residues in the sequence. [d]KLVFFAK was also found in Aβ Italian mutation.

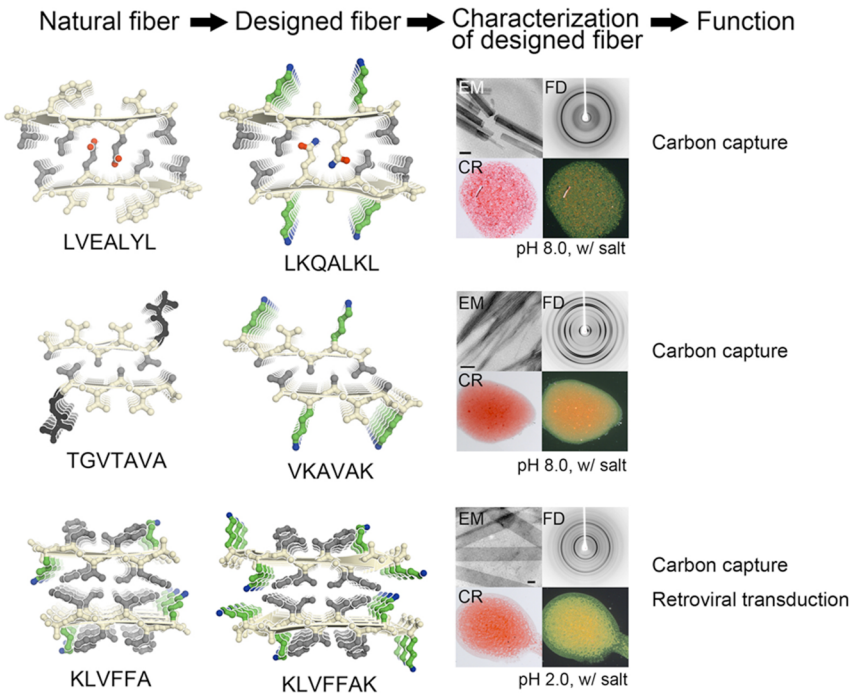

Figure 2. Three examples of fiber design and characterization. From LVEALYL to LKQALKL: residue Glu of LVEALYL was changed to Gln. The natural, fiber-forming segment LVEALYL can only form fibers when the carboxyl group (oxygen atoms are in red) of Glu is neutral. The designed peptide in which Gln replaces Glu may form fibers under a wide range of pH. Two lysines (side chain carbons are in green and nitrogen is in blue) were added by replacing Val and Tyr, which face out from the zipper spine. EM, FD, and CR staining prove the formation of designed amyloid fibers. From TGVTAVA to VKAVAK: Thr and Gly (black) of TGVTAVA were cut off because they are not in the zipper spine. Lysines were added by substituting the second Thr and Ala residues. From KLVFFA to KLVFFAK: KLVFFA forms antiparallel fibers. LVFF is necessary to form the zipper spine and is not available for functionalization. KLVFFA contains one lysine, therefore a second lysine was added to the C-terminus. Side chains of amino acids that form the zipper spines are in gray. The scale bars of EM images are 500 nm.

processed by smoothing and subtraction of the blank according to the manufacturer's specified protocol.

6. Congo Red Staining. Fibers were spun down at 20000*g*. Pellets were resuspended in 100 μL of 0.1 mg mL^{-1} Congo red dissolved in 10 mM Tris pH 8.0, 0.15 M NaCl, and incubated for 30 min at room temperature. They were centrifuged again at 20000*g*. Pellets were resuspended in 100 μL of water. This was repeated until the supernatant ceased to be red. Pellets were finally resuspended with 5−7 μL of water and dropped on a glass coverslip to be dried at room temperature. Stains were examined with a ZEISS SteREO Discovery V20 microscope under normal and polarized lights.

7. Fiber X-ray Diffraction. Fiber pellets were washed with water twice via centrifugation and resuspension. Fibers were suspended with 5 μL of water afterward. The suspension was pipetted between two fire-polished glass rods until dry. Glass rods with dry fibers were mounted on an in-house X-ray machine equipped with Rigaku FR-D X-ray generator and ADSC-Quantum4 CCD detector. Diffraction images were collected using a 5° oscillation with 5 min exposures.

8. Breakthrough Experiment. A laboratory-made breakthrough system was used to evaluate dynamic carbon dioxide selectivity over nitrogen. Adsorbent materials were packed in stainless steel Swagelok tubing (4 mm i.d. × 50 mm). Volume not occupied by the adsorbent bed was filled with glass beads (Sigma, 150−212 μm). The gas feed stream mixed 16% carbon dioxide in nitrogen for separation, and 100% nitrogen for regeneration, which was determined by MKS Alta digital mass flow controllers. The pressure was held at 760 Torr by an MKS Type 640 pressure controller. The gaseous effluent from the sample bed was monitored for carbon dioxide, nitrogen, water, and oxygen by using a mass spectrometer (Hiden Analytical HPR20). In the process

dx.doi.org/10.1021/ja509648u | J. Am. Chem. Soc. 2014, 136, 18044−18051

of regeneration, the material bed was heated to 100 °C with nitrogen purging.

9. Transduction/Infection Assay. First, 50−60% confluent HEK293T cells seeded in 24-well plates were infected with a solution comprising 150 μL of virus particles containing medium, 350 μL of DMEM/10% FBS fresh medium, and different concentrations of fiber suspension. The fluorescent cell images were taken 48 h later, and the efficiency of transduction/infection was then quantified by FACs analysis of the percentage of the GFP positive cells.

RESULTS

1. Procedure for Structure-Based Functionalization of Amyloid Fibers. Our procedure for structure-based design of functional amyloid fibers is illustrated in Figure 1. Atomic structures have shown that amyloid-forming peptides assemble into amyloid fibers via backbone hydrogen-bond interactions forming β-sheets and sequence-specific side-chain interactions zipping the sheets into a pair. The compact fibrillar structure determined by X-ray crystallography is coined the "steric zipper" because the side chains interdigitate like the teeth of a zipper.[37,38] So far, there are ∼120 unique steric-zipper structures in our zipper structure database (Figure 1a). β-sheets pack either parallel or antiparallel, with most having β-strands in-register but some with strands out of register. The variety of steric-zipper structures offers a diverse repertoire of templates for functional design. We have learned from structures that the inward-facing side chains form the "teeth" of the zipper, causing the β-sheet pairs to zip up, forming the fiber spine (Figure 1b). Therefore, outward- facing side chains are available for engineering functionalities. While the sequence variation of the fiber-forming segment is limited, functionality can be added by extending the length of peptides with

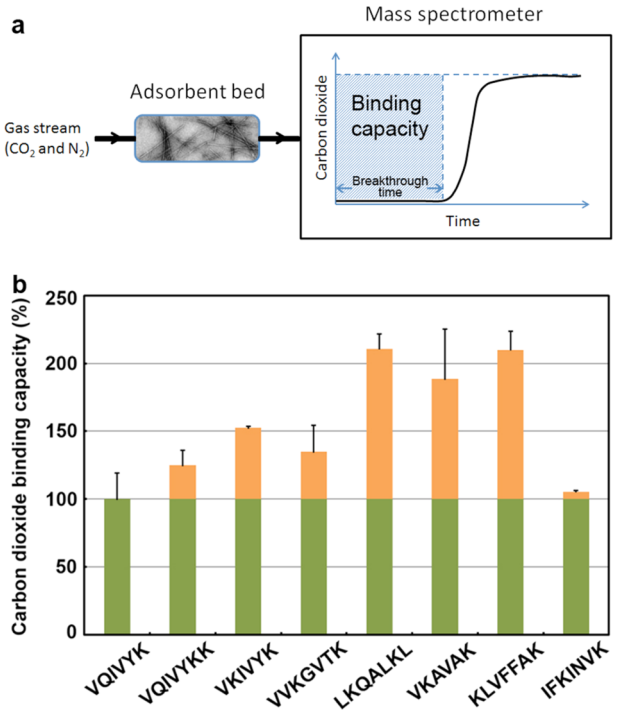

Figure 3. Dynamic carbon dioxide binding capacity of designed fibers measured by breakthrough experiments. (a) Illustration of a breakthrough measurement. A gas stream composed of 16% carbon dioxide and 84% nitrogen is fed through the adsorbent bed filled with amyloid material. The outflow gas is monitored by mass spectrometry. As the material adsorbs carbon dioxide, a lag of carbon dioxide signal is observed. The lag time is called the breakthrough time representing the dynamic binding capacity of the material. (b) Comparison of carbon dioxide capacity of designed fibers with that of the natural VQIVYK fiber. Data of VQIVYKK and VKIVYK are from ref 24. Designed fibers are formed under their unique optimal conditions for carbon dioxide binding, as described in the text. Directly comparable results for fibers formed under other conditions are shown in SI Figure S5.

Table 2. Summary of Our Peptide Designs for Retroviral Transduction

		fibrillation condition		
name	sequence	pH	salt	fold of infection rate[a]
VIBA1a	KLVFFAK	2.0	−	1.4 ± 0.3
VIBA1b	KLVFFAK	8.0	−	1.3 ± 0.2
VIBA1c	KLVFFAK	2.0	+	2.8 ± 0.2
VIBA2a	KKKVQIVYK	8.0	−	1.1 ± 0.2
VIBA2b	KKKVQIVYK	12.0	−	1.4 ± 0.1
VIBA2c	KKKVQIVYK	12.0	+	1.2 ± 0.1
VIBA3	VQIVYKK	8.0	+	1.9 ± 0.3
VIBA4	RLVFFAR	2.0	−	2.0 ± 0.4
VIBA5	RLVFFAK	2.0	−	1.8 ± 0.1
VIBA6	LKQALKL	8.0	+	1.2 ± 0.0

[a]"Virus only" is 1.0. Values are from the best working concentration of fibers.

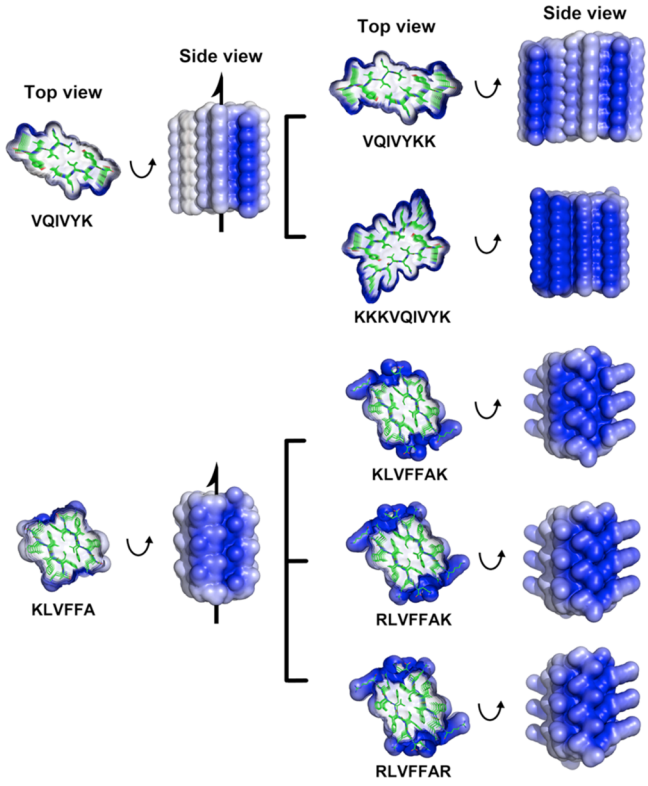

Figure 4. Electrostatic surface potential of models of designed amyloid steric zippers for retroviral transduction. Each steric-zipper block shows seven β-strands in each sheet. The fiber spines of VQIVYK and KLVFFA present lysines in different patterns on the zipper surface. Addition of lysine or arginine residues raises the surface positive charge, which may consequently enhance their facilitation of retroviral transduction. Electrostatic surfaces were calculated using APBS[48] based on the experimental and modeled structures. Straight arrows indicate the fiber axes.

dx.doi.org/10.1021/ja509648u | J. Am. Chem. Soc. 2014, 136, 18044−18051

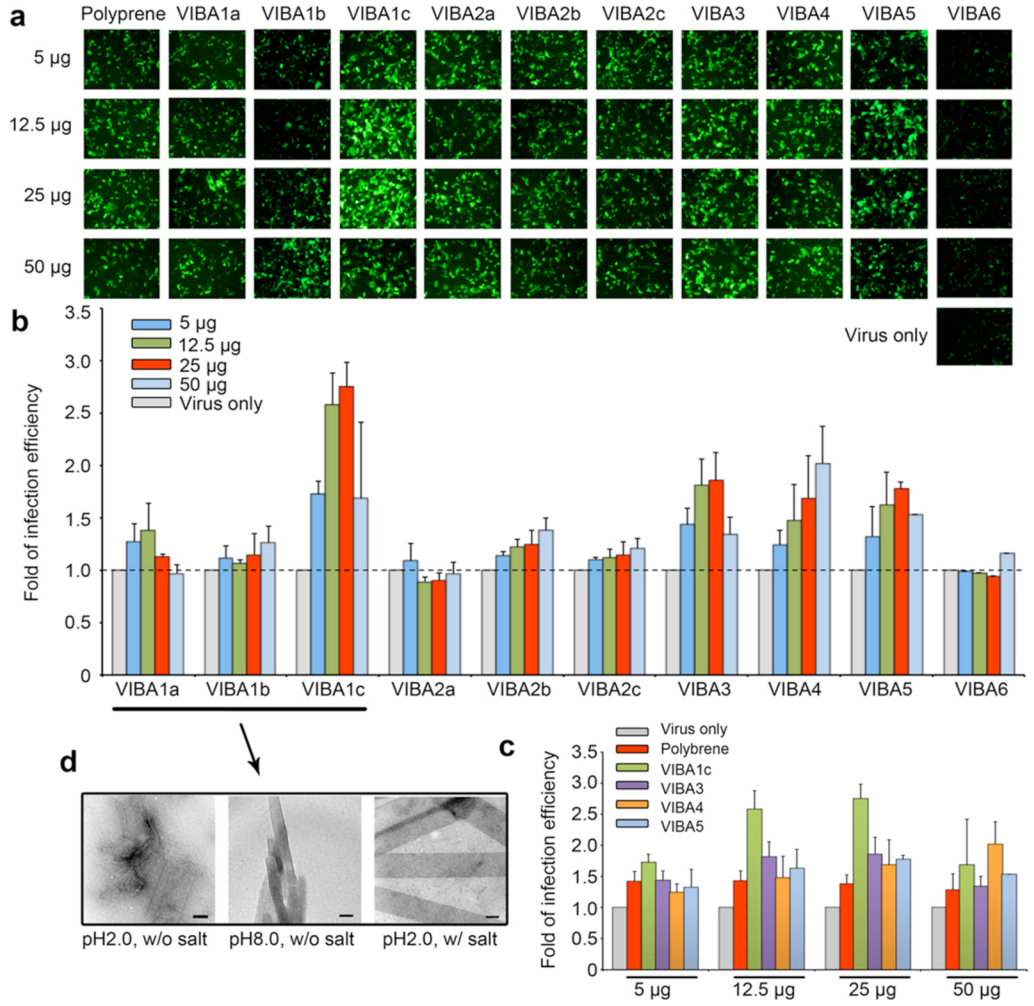

Figure 5. Designed amyloid fibers enhance lentiviral transduction. (a) Human 293T cells transduced (GFP+) with various fiber-treated lentivirus. (b) Effect of designed fibers on lentiviral gene transfer into 293T cells. VIBAs 1c, 3, 4, and 5 showed significant enhancement of infection efficiency. (c) The efficiency of VIBAs 1c, 3, 4, and 5 compares favorably with polybrene. (d) EM images of VIBA1 fibers formed under different conditions showing polymorphism, which results in different efficiencies of virion transduction. The scale bars are 200 nm.

functional residues (Figure 1c). The amyloid-forming peptides in our database are segments of natural proteins that form amyloid. These segments are capable of forming amyloid fibers in isolation from the rest of their parent proteins, as well as inducing fiber formation upon introduction into a non-amyloidogenic protein[39,40] Therefore, starting from the spine sequence, the segment peptide can be theoretically extended with additional residues without losing its capacity to form fibers.

2. Application 1: Environmental Carbon Dioxide Capture. *2.1. Fiber Design.* We have previously introduced the use of amyloid fibers for carbon dioxide capture as a step toward addressing the global threat of climate change.[24] The fibers were formed by a natural hexapeptide VQIVYK, the key amyloid-forming segment of Tau protein. The binding of carbon dioxide occurs via carbamate formation with lysine residues. Compared with the state-of-the-art solid materials including zeolites and metal−organic frameworks (MOFs), the selectivity of carbon dioxide on this new material, in powdered form, does not drop even in the presence of water vapor, the other principal component of combustion, so that this material is promising for selective extraction of carbon dioxide from combustion gases. However, the capacity of our previously described amyloid material is only half of Mg-MOF-74, the benchmark MOF molecule.[41] In this work, we aim to double the binding capacity by designing fibers with double the density of lysine residues.

In our designs, we screened parameters such as geometry, buried surface area, shape complementarity (Sc) of the zipper spine, solubility, pH sensitivity, fiber yield, and lysine spacing (Table 1). We chose seven zipper spines from our database of structures. Among them, the atomic structures of IFQINS from lysozyme, and TGVTAVA and VVTGVTA from α-synuclein are first reported in this work (SI Table S1). Six of them are parallel β-sheets like the original fiber, VQIVYK, but have significantly larger buried surface and Sc causing these peptides to form tighter fiber spines. We also chose the peptide KLVFFA featuring antiparallel sheets. Along the fiber axis, lysines are separated by 4.8 Å in parallel fibers and 9.6 Å in antiparallel fibers. Because carbamate, the reaction product, is negatively charged, greater separation between lysines may help to stabilize the reaction.

Residues with side chains oriented toward the mating sheet form the zipper spine essential to drive fiber assembly. To increase fiber yield, we optimized zipper spines to have lower solubility without changing their complementarity (Table 1,

dx.doi.org/10.1021/ja509648u | J. Am. Chem. Soc. 2014, 136, 18044−18051

Figure 2, and SI Figure S1). For example, the residue Ser of the peptide IFQINS was replaced by Val, and Asn of NKGAII was replaced by Ile. Val and Ile are hydrophobic residues, and of similar size to Ser and Asn, respectively. Therefore, the designed peptides have lower solubility and are more prone to aggregation. We also optimized the zipper spine for higher pH tolerance. Peptide LVEALYL is sensitive to pH because the residue Glu must be neutral in order to form the zipper spine, which requires low pH. We replaced Glu with Gln, so the peptide can form fibers over a wide pH range. Finally, to double carbon dioxide binding capacity, we added two lysines to each peptide, and separated them in the sequence. For comparison, we also designed VQIVYKK with two adjacent lysines.

2.2. Fiber Formation. To find the condition for fiber formation of each peptide, we screened acidic (2.0), near neutral (8.0), and basic (12.0) pH values with and without salt. After incubation, amyloid fiber formation was characterized by electron microscopy (EM), circular dichroism (CD), Congo red (CR) staining, and fiber X-ray diffraction (FD) (Figure 2, SI Figures S1 and S2). We note that fiber yield is positively correlated with peptide hydrophobicity (Table 1 and SI Figure S3). Peptides IFKINVK and KLVFFAK fibrillate extensively under nearly all conditions. These two peptides are the most hydrophobic. In contrast, the most hydrophilic peptides KNNQKNY and NKGAIK barely form fibers. In addition, LKQALKL is able to form fibers at alkaline pH by substituting the residue Glu in the original peptide with Gln. Polymorphism has been observed in both peptide and protein fibers.[42−44] We also observe polymorphism in designed peptides. Under different conditions, all peptides, except for NKGAIK, which does not form fibers under tested conditions, form amyloid fibers with various morphologies (SI Figure S4). We observed fibers that are straight, twisted, crystal-like, tape-like, and tube-like in appearance. Their width ranges from 20 to 400 nm, and length ranges from 100 nm to several μm. Furthermore, many peptides only form fibers under certain conditions. The variability of conditions controlling fiber formation and morphology indicates a tunable property of amyloid, which is favorable for applications like biosensors and nanoelectronic switches. Nine of ten designed peptides formed amyloid fibers, demonstrating the reliability of the design method. As controls, we also synthesized peptides VTKVAK (compared to VKAVAK) and VKTGVTK (compared to VVKGVTK) with lysines breaking the zipper spine. As expected, they do not form fibers, which reinforces the steric-zipper hypothesis.

2.3. Designed Fibers Double the Carbon Dioxide Binding Capacity. Dynamic separation of carbon dioxide from flue exhaust is a more relevant metric for real-world applications than static thermodynamic uptake capacity. We measured and compared carbon dioxide binding capacity of designed fibers with the natural VQIVYK fiber by using breakthrough experiments that directly measure dynamic separation capacity (Figure 3). The method has been described previously.[24,41] In brief, to mimic the carbon dioxide composition of power plant flue gas, we mixed 16% carbon dioxide into a nitrogen gas stream through the material and detected the "breakthrough" time of carbon dioxide from the material (Figure 3a). The results show that three designed fibers, LKQALKL, VKAVAK, and KLVFFAK, succeeded in doubling the capacity of VQIVYK (Figure 3b), validating our method of structure-based amyloid design.

2.4. Factors That Matter. We notice that fibers formed by the same peptide under different conditions have different carbon dioxide capacities (SI Figure S5). Binding capacity is not solely determined by the number of lysines, but also by the reactivity and accessibility of their ε-amino groups. We can theoretically add many lysines to a peptide, but they may not function optimally. For example, VQIVYKK works poorly with two adjacent lysines at one end. Lysine spacing is important for the accessibility of amino groups. The space of lysines is not only determined by their relative positions in the fiber spine, but ultimately in mature fibers. Our fiber models are based on the zipper structure of peptides with just a single pair of β-sheets, which represents the structure of fiber spine. However, mature fibers are formed by many pairs of β-sheets and may involve in higher order of assembly into clusters or plaques. The steric distance of lysines may get close in the mature fiber, even though they are distant in the fiber spine. Therefore, the function testing of the designed fiber is not only a proof and also a screening and optimization of the fiber design. In summary, for carbon dioxide capture, peptide hydrophobicity is important to ensure a high yield of fibers, and lysine spacing is important for fiber reactivity.

3. Application 2: Retroviral Transduction. *3.1. Fiber Design.* Amyloid fibers boost retroviral transduction found in HIV infection by semen-derived SEVI fibers[45] and in laboratorial gene transfer by HIV-1 gp120-derived EF-C (QCKIKQIINMWQ) fibers.[23] The underlying mechanism has been postulated to involve electrostatic attraction: the positively charged fibers mediate the interaction between negatively charged viral and cellular membranes, thus suggesting the possibility of enhancing retroviral transduction in basic research and clinical applications.[23,45,46]

According to this postulated mechanism, we incorporated various numbers of lysines in the peptides (Table 2). Given that arginine has a higher pK_a than lysine, we also incorporate arginine in some designs. In the design for viral transduction, we chose one parallel spine, VxIxY of VQIVYK and one antiparallel spine, LVFF of KLVFFA to examine different charge patterns (Figure 4). Aside from assembly geometry, we also tested fibers formed by the same peptide but under different solution conditions, respectively, in consideration of fiber polymorphism (described above and in SI Figure S4).

3.2. Fiber Formation. All designed peptides form amyloid fibers confirmed by EM, CR, and FD (Figure 2 and SI Figure S1), which again proves that fiber spines suffice for fiber formation. Notably, KKKVQIVYK forms fibers under many conditions despite being highly soluble in water (hydrophobicity = −0.34[47]), suggesting that the terminal extension of the peptide beyond the fiber spine has little effect on the fiber yield. This observation is consistent with the fact that in natural proteins the insertion of fiber spines as short as six amino acids can cause fibrillation of full-length proteins as long as hundreds of amino acids.[39,40]

3.3. Designed Fibers Triple Retroviral Transduction Efficiency. We tested the designed fibers for enhancement of lentivirus infection of human 293T cells. We found that the designed fibers with positively charged residues generally increased the efficiency of lentivirus gene transfer (Figure 5). We name these fibers "viral infection boosting amyloids" (VIBAs). Among them, VIBAs 1c, 3, 4, and 5 significantly boosted the viral transduction rate. Notably, VIBA1c nearly triples the efficiency. The efficacy of VIBAs increases in a dose-dependent manner, though cytotoxicity is observed at the highest concentrations of some fibers. Compared with polyprene, a popular transduction enhancer, VIBA1c is two

times more efficient (Figure 5c). The designed peptides are much shorter than the previously reported SEVI fiber and gp120 EF-C fiber, thus less expensive. More importantly, the scaffold can be easily adapted to optimize design methodology and improve fiber performance.

3.4. Factors That Matter. Fiber morphology is closely related to the efficacy of fibers in boosting retroviral transduction. We notice that for the same sequence, fibers obtained under different conditions showed significant variation in facilitating cell infection (Table 2 and Figure 5). In mediating retroviral transduction, different morphologies may display different surfaces for virion adhesion. Fiber designs based on both parallel and antiparallel spines show no significant differences. And extension with lysines as in samples of VIBA 2 (KKKVQIVYK) has no obvious improvement. Both designed fibers containing arginine, VIBAs 4 and 5, showed significant enhancement of virion transduction. Although the effect is not as strong as VIBA1c, VIBA4 is much less toxic to the cells at high concentration. Notably, KLVFFAK is one of the most effective designs in both carbon capture and virion transduction boosting, which is conceivable because the two applications both use lysine as the functional residue. In contrast, the LKQALKL fiber, which is as effective as the KLVFFAK fiber in carbon capture showed little effect in retroviral transduction (Figures 3b and 5a,b). In both applications, the ε-amino group of lysine must be accessible to function. However, carbon dioxide is much smaller than virion particles. So lysines need to be on more widely opened surfaces for virion attachment than for carbon dioxide interaction.

We have applied structure-based design of amyloid fibers in two very diverse applications: environmental carbon dioxide capture and enhancing retroviral gene transduction. The weight of factors is different in the two cases even for the same functional group. The evaluation of different factors will guide the optimization of future designs. For further applications, for example amyloid nanowires, properties such as shape, size, homogeneity, and strength may be more relevant. Therefore, design strategies for diverse applications should employ a variety of fiber spines and fibrillation conditions.

CONCLUSION

We present a methodology for structure-based functionalization of amyloid fibers as materials. We show that designed peptides based on their steric-zipper structures have a high success rate for producing artificial amyloid fibers. The designed fibers gain applicable functions upon incorporation of reactive, properly positioned amino acids. In one model system, we designed fibers that double the carbon dioxide binding capacity of the natural VQIVYK fiber for environmental carbon capture, and another system triples the efficiency of lentivirion cell infection. Moreover, these design principles can be adopted to create a vast array of robust new materials with diverse functions.

ASSOCIATED CONTENT

Supporting Information

Table of crystallographic information on peptides IFQINS, TGVTAVA, and VVTGVTA; figures including structure models and characterization of design fibers, amyloid fiber formation efficiency of designed peptides, various morphologies of designed fibers, and the relation of morphology and function. This material is available free of charge via the Internet at http://pubs.acs.org.

AUTHOR INFORMATION

Corresponding Author

david@mbi.ucla.edu

Present Addresses

[#]M.I.: Department of Neurology, University of Michigan Medical School, Ann Arbor, MI 48109

[▽]S.A.S.: Division of Biology and Biological Engineering, California Institute of Technology, Pasadena, CA 91125

Notes

The authors declare no competing financial interest.

ACKNOWLEDGMENTS

This work was supported by DOE cooperative agreement DE-FCO-02ER-63421 and NSF MCB 0958111. C.L. acknowledges the financial support from the Chinese Academy of Sciences and the 1000 Talents Program, China. We thank Electron Imaging Center for NanoMachines of California NanoSystems Institute (CNSI) at UCLA, and National Center for Protein Science (Shanghai) for using TEM. We thank Christian Riekel, Manfred Burghammer, the staff at the European Synchrotron Radiation Facility, beamline ID-13, Anders Madsen, and Marcin Apostol for their roles in microcrystal X-ray diffraction data collection.

REFERENCES

(1) Goldschmidt, L.; Teng, P. K.; Riek, R.; Eisenberg, D. *Proc. Natl. Acad. Sci. U.S.A.* **2010**, *107*, 3487−3492.

(2) Dobson, C. M. *Nature* **2003**, *426*, 884−890.

(3) Adamcik, J.; Jung, J.-M.; Flakowski, J.; De Los Rios, P.; Dietler, G.; Mezzenga, R. *Nat. Nanotechnol.* **2010**, *5*, 423−428.

(4) Fitzpatrick, A. W.; Debelouchina, G. T.; Bayro, M. J.; Clare, D. K.; Caporini, M. A.; Bajaj, V. S.; Jaroniec, C. P.; Wang, L.; Ladizhansky, V.; Müller, S. A.; MacPhee, C. E.; Waudby, C. A.; Mott, H. R.; De Simone, A.; Knowles, T. P.; Saibil, H. R.; Vendruscolo, M.; Orlova, E. V.; Griffin, R. G.; Dobson, C. M. *Proc. Natl. Acad. Sci. U.S.A.* **2013**, *110*, 5468−5473.

(5) Eisenberg, D.; Jucker, M. *Cell* **2012**, *148*, 1188−1203.

(6) Liu, C.; Zhao, M.; Jiang, L.; Cheng, P.-N.; Park, J.; Sawaya, M. R.; Pensalfini, A.; Gou, D.; Berk, A. J.; Glabe, C. G.; Nowick, J.; Eisenberg, D. *Proc. Natl. Acad. Sci. U.S.A.* **2012**, *109*, 20913−20918.

(7) Knowles, T. P.; Buehler, M. J. *Nat. Nanotechnol.* **2011**, *6*, 469−479.

(8) Fitzpatrick, A. W.; Park, S. T.; Zewail, A. H. *Proc. Natl. Acad. Sci. U.S.A.* **2013**, *110*, 10976−10981.

(9) Cherny, I.; Gazit, E. *Angew. Chem., Int. Ed.* **2008**, *47*, 1521−3773.

(10) Li, C.; Mezzenga, R. *Nanoscale* **2013**, *5*, 6207−6218.

(11) Mankar, S.; Anoop, A.; Sen, S.; Maji, S. K. *Nano Rev.* **2011**, *2*, 6032.

(12) Holmes, T. C.; de Lacalle, S.; Su, X.; Liu, G.; Rich, A.; Zhang, S. *Proc. Natl. Acad. Sci. U.S.A.* **2000**, *97*, 6728−6733.

(13) Gras, S. L.; Tickler, A. K.; Squires, A. M.; Devlin, G. L.; Horton, M. A.; Dobson, C. M.; MacPhee, C. E. *Biomaterials* **2008**, *29*, 1553−1562.

(14) Maji, S. K.; Schubert, D.; Rivier, C.; Lee, S.; Rivier, J. E.; Riek, R. *PLoS Biol.* **2008**, *6*, No. e17.

(15) Bhak, G.; Lee, S.; Park, J. W.; Cho, S.; Paik, S. R. *Biomaterials* **2010**, *31*, 5986−5995.

(16) Koutsopoulos, S.; Unsworth, L. D.; Nagai, Y.; Zhang, S. *Proc. Natl. Acad. Sci. U.S.A.* **2009**, *106*, 4623−4628.

(17) Raynes, J. K.; Pearce, F. G.; Meade, S. J.; Gerrard, J. A. *Biotechnol. Prog.* **2011**, *27*, 360−367.

(18) Scheibel, T.; Parthasarathy, R.; Sawicki, G.; Lin, X. M.; Jaeger, H.; Lindquist, S. L. *Proc. Natl. Acad. Sci. U.S.A.* **2003**, *100*, 4527−4532.

(19) Reches, M.; Gazit, E. *Science* **2003**, *300*, 625−627.

(20) Chen, A. Y.; Deng, Z.; Billings, A. N.; Seker, U. O.; Lu, M. Y.; Citorik, R. J.; Zakeri, B.; Lu, T. K. *Nat. Mater.* **2014**, *13*, 515−523.

(21) Knowles, T. P.; Oppenheim, T. W.; Buell, A. K.; Chirgadze, D. Y.; Welland, M. E. *Nat. Nanotechnol.* **2010**, *5*, 204−207.
(22) Channon, K. J.; Devlin, G. L.; MacPhee, C. E. *J. Am. Chem. Soc.* **2009**, *131*, 12520−12521.
(23) Yolamanova, M.; Meier, C.; Shaytan, A. K.; Vas, V.; Bertoncini, C. W.; Arnold, F.; Zirafi, O.; Usmani, S. M.; Muller, J. A.; Sauter, D.; Goffinet, C.; Palesch, D.; Walther, P.; Roan, N. R.; Geiger, H.; Lunov, O.; Simmet, T.; Bohne, J.; Schrezenmeier, H.; Schwarz, K.; Standker, L.; Forssmann, W. G.; Salvatella, X.; Khalatur, P. G.; Khokhlov, A. R.; Knowles, T. P.; Weil, T.; Kirchhoff, F.; Munch, J. *Nat. Nanotechnol.* **2013**, *8*, 130−136.
(24) Li, D.; Furukawa, H.; Deng, H.; Liu, C.; Yaghi, O. M.; Eisenberg, D. *Proc. Natl. Acad. Sci. U.S.A.* **2014**, *111*, 191−196.
(25) Rufo, C. M.; Moroz, Y. S.; Moroz, O. V.; Stohr, J.; Smith, T. A.; Hu, X.; Degrado, W. F.; Korendovych, I. V. *Nat. Chem.* **2014**, *6*, 303−309.
(26) Li, J.; McQuade, T.; Siemer, A. B.; Napetschnig, J.; Moriwaki, K.; Hsiao, Y. S.; Damko, E.; Moquin, D.; Walz, T.; McDermott, A.; Chan, F. K.; Wu, H. *Cell* **2012**, *150*, 339−350.
(27) Kato, M.; Han, T. W.; Xie, S.; Shi, K.; Du, X.; Wu, L. C.; Mirzaei, H.; Goldsmith, E. J.; Longgood, J.; Pei, J.; Grishin, N. V.; Frantz, D. E.; Schneider, J. W.; Chen, S.; Li, L.; Sawaya, M. R.; Eisenberg, D.; Tycko, R.; McKnight, S. L. *Cell* **2012**, *149*, 753−767.
(28) Majumdar, A.; Cesario, W. C.; White-Grindley, E.; Jiang, H.; Ren, F.; Khan, M. R.; Li, L.; Choi, E. M.; Kannan, K.; Guo, F.; Unruh, J.; Slaughter, B.; Si, K. *Cell* **2012**, *148*, 515−529.
(29) Maji, S. K.; Perrin, M. H.; Sawaya, M. R.; Jessberger, S.; Vadodaria, K.; Rissman, R. A.; Singru, P. S.; Nilsson, K. P.; Simon, R.; Schubert, D.; Eisenberg, D.; Rivier, J.; Sawchenko, P.; Vale, W.; Riek, R. *Science* **2009**, *325*, 328−332.
(30) Blanco, L. P.; Evans, M. L.; Smith, D. R.; Badtke, M. P.; Chapman, M. R. *Trends Microbiol.* **2012**, *20*, 66−73.
(31) Hauser, C. A. E.; Maurer-Stroh, S.; Martins, I. C. *Chem. Soc. Rev.* **2014**, *43*, 5326−5345.
(32) Riekel, C. *J. Synchrotron Radiat.* **2004**, *11*, 4−6.
(33) Otwinowski, Z.; Minor, W. *Methods Enzymol.* **1997**, *276*, 307−326.
(34) McCoy, A. J.; Grosse-Kunstleve, R. W.; Storoni, L. C.; Read, R. J. *Acta Crystallogr. D: Biol. Crystallogr.* **2005**, *61*, 458−464.
(35) Emsley, P.; Cowtan, K. *Acta Crystallogr. D: Biol. Crystallogr.* **2004**, *60*, 2126−2132.
(36) Murshudov, G. N.; Vagin, A. A.; Dodson, E. J. *Acta Crystallogr. D: Biol. Crystallogr.* **1997**, *53*, 240−255.
(37) Sawaya, M. R.; Sambashivan, S.; Nelson, R.; Ivanova, M. I.; Sievers, S. A.; Apostol, M. I.; Thompson, M. J.; Balbirnie, M.; Wiltzius, J. J.; McFarlane, H. T.; Madsen, A. O.; Riekel, C.; Eisenberg, D. *Nature* **2007**, *447*, 453−457.
(38) Nelson, R.; Sawaya, M. R.; Balbirnie, M.; Madsen, A. O.; Riekel, C.; Grothe, R.; Eisenberg, D. *Nature* **2005**, *435*, 773−778.
(39) Teng, P. K.; Anderson, N. J.; Goldschmidt, L.; Sawaya, M. R.; Sambashivan, S.; Eisenberg, D. *Protein Sci.* **2012**, *21*, 26−37.
(40) Sambashivan, S.; Liu, Y.; Sawaya, M. R.; Gingery, M.; Eisenberg, D. *Nature* **2005**, *437*, 266−269.
(41) Britt, D.; Furukawa, H.; Wang, B.; Glover, T. G.; Yaghi, O. M. *Proc. Natl. Acad. Sci. U.S.A.* **2009**, *106*, 20637−20640.
(42) Wiltzius, J. J.; Landau, M.; Nelson, R.; Sawaya, M. R.; Apostol, M. I.; Goldschmidt, L.; Soriaga, A. B.; Cascio, D.; Rajashankar, K.; Eisenberg, D. *Nat. Struct. Mol. Biol.* **2009**, *16*, 973−978.
(43) Petkova, A. T.; Leapman, R. D.; Guo, Z.; Yau, W. M.; Mattson, M. P.; Tycko, R. *Science* **2005**, *307*, 262−265.
(44) Colletier, J. P.; Laganowsky, A.; Landau, M.; Zhao, M.; Soriaga, A. B.; Goldschmidt, L.; Flot, D.; Cascio, D.; Sawaya, M. R.; Eisenberg, D. *Proc. Natl. Acad. Sci. U.S.A.* **2011**, *108*, 16938−16943.
(45) Munch, J.; Rucker, E.; Standker, L.; Adermann, K.; Goffinet, C.; Schindler, M.; Wildum, S.; Chinnadurai, R.; Rajan, D.; Specht, A.; Gimenez-Gallego, G.; Sanchez, P. C.; Fowler, D. M.; Koulov, A.; Kelly, J. W.; Mothes, W.; Grivel, J. C.; Margolis, L.; Keppler, O. T.; Forssmann, W. G.; Kirchhoff, F. *Cell* **2007**, *131*, 1059−1071.
(46) Usmani, S. M.; Zirafi, O.; Müller, J. A.; Sandi-Monroy, N. L.; Yadav, J. K.; Meier, C.; Weil, T.; Roan, N. R.; Greene, W. C.; Walther, P.; Nilsson, K. P.; Hammarström, P.; Wetzel, R.; Pilcher, C. D.; Gagsteiger, F.; Fändrich, M.; Kirchhoff, F.; Münch, J. *Nat. Commun.* **2014**, *5*, 3508.
(47) Eisenberg, D.; Schwarz, E.; Komaromy, M.; Wall, R. *J. Mol. Biol.* **1984**, *179*, 125−142.
(48) Baker, N. A.; Sept, D.; Joseph, S.; Holst, M. J.; McCammon, J. A. *Proc. Natl. Acad. Sci. U.S.A.* **2001**, *98*, 10037−10041.